Cross calibration of ocean-color bands from Moderate Resolution Imaging Spectroradiometer on Terra platform

Ewa J. Kwiatkowska,[1,2,*] Bryan A. Franz,[1,2] Gerhard Meister,[1,3] Charles R. McClain,[1] and Xiaoxiong Xiong[4]

[1]Ocean Biology Processing Group, 614.8, National Aeronautics and Space Administration, Goddard Space Flight Center, Maryland 20771, USA

[2]Science Applications International Corporation, Beltsville, Maryland 20705, USA

[3]Futuretech Corporation, Greenbelt, Maryland 20770, USA

[4]Moderate Resolution Imaging Spectroradiometer Characterization Support Team, National Aeronautics and Space Administration, Goddard Space Flight Center, Maryland 20771, USA

*Corresponding author: ewa.kwiatkowska@gmail.com

Received 26 June 2008; revised 18 October 2008; accepted 18 October 2008; posted 21 October 2008 (Doc. ID 98002); published 15 December 2008

Ocean-color applications require maximum uncertainties in blue-wavelength water-leaving radiances in oligotrophic ocean of approximately 5%. Water-leaving radiances from Moderate Resolution Imaging Spectroradiometer (MODIS) on the Terra satellite, however, exhibit temporal drift of the order of 15% as well as sensor changes in response versus scan and polarization sensitivity, which cannot be tracked by onboard calibrators. This paper introduces an instrument characterization approach that uses Earth-view data as a calibration source. The approach models the top of the atmosphere signal over ocean that the instrument is expected to measure, including its polarization, with water-leaving radiances coming from another well-calibrated global sensor. The cross calibration allows for significant improvement in derived MODIS–Terra ocean-color products, with largest changes in the blue wavelengths.

OCIS codes: 010.0280, 010.1690, 010.1285, 010.4450, 280.4788.

1. Introduction

Satellite monitoring of phytoplankton pigments in the near-surface water layers has revealed the enormous impact the oceanic plankton have on global carbon dioxide fixation and Earth's climate [1]. These space sensors operate in the visible and near-infrared range of the electromagnetic spectrum, thus derived data are called ocean color. The instruments measure radiance exiting the top of the atmosphere (TOA) at a number of discrete wavelengths. The algorithms in routine use make the assumption that the atmospheric and oceanic components of the TOA radiance (L_t) can be largely decoupled using theoretical models of radiative transfer and that the atmospheric absorption and scattering can also be separated [2–4]. The spectral distribution of upwelling visible light is derived just above the ocean surface and is referred to as the water-leaving radiance (L_w). Water-leaving radiances are subsequently used to calculate biophysical properties of the ocean, including concentrations of phytoplankton photosynthetic pigment, chlorophyll-a (C_a). More than 75% of the world's oceans are covered by oligotrophic waters where chlorophyll-a concentrations are below $0.1\,\mathrm{mg/m^3}$ [5]. Because of intense atmospheric scattering by air molecules and aerosols and strong

0003-6935/08/366796-15$15.00/0

water absorption, water-leaving radiances in oligotrophic ocean contribute only approximately 17% to the TOA radiance in the blue and 8% in the green spectral wavelengths [5]. At the near-infrared range, water-leaving radiances in the oligotrophic regime are assumed negligible, and all TOA radiance is attributed to atmospheric scattering and absorption. Because of the low magnitude of the ocean contribution and uncertainties in the atmospheric correction, accurate characterization and calibration of ocean-color sensors is vital.

Sea-viewing Wide Field-of-View Sensor (SeaWiFS) on the OrbView-2 satellite [6] and Moderate Resolution Imaging Spectroradiometers (MODISs) [7] flying on the Terra and Aqua spacecraft have been capturing global ocean-color data since 1997, 2000, and 2002, respectively. SeaWiFS is solely dedicated to ocean-color observations and carries eight bands from the blue, 412 nm, to the near-infrared, 865 nm, range of the spectrum. MODIS has 36 spectral bands from the blue, 412 nm, to the thermal infrared, 14.235 μm, from which nine bands have the wavelength and the radiometric sensitivity required for ocean-color applications. The calibration process for these instruments is complex. Direct methods include comprehensive prelaunch characterizations and on-orbit calibrations using onboard calibration sources and the Moon [8–10]. Total uncertainties of direct absolute radiance calibrations are similar between SeaWiFS and MODIS instruments and add up to 5% [8,11]. The goal of ocean color is to estimate oligotrophic water-leaving radiances in blue wavelengths to within 5% error [12]. However, the total uncertainties from sensor direct calibrations introduce up to 30% uncertainty in water-leaving radiances. To reduce these uncertainties, additional vicarious calibrations are implemented [13].

SeaWiFS has been a well-calibrated source of ocean-color data for over 10 years [14], and MODIS–Aqua water-leaving radiances currently agree with SeaWiFS to within 5% on the global average [15]. In contrast, Franz *et al.* demonstrated in detail that MODIS–Terra is currently unsuitable for quantitative ocean-color applications [5]. In summary, they found that ocean-color products from Terra exhibit a significant temporal drift of approximately 15% that can be attributed to increased instrument degradation and that resulting changes in MODIS response versus scan angle (RVS) and polarization sensitivity cannot be readily tracked by onboard calibrators. The shape of the MODIS RVS is fixed at prelaunch laboratory measurements and is linearly scaled based on two reference points corresponding to two independent on-orbit calibration procedures using solar diffuser (SD) and lunar observations [16]. The two calibration points are obtained when the MODIS double-sided scan mirror observes the SD at a 50.3° angle of incidence (AOI), equivalent to Earth-view (EV) pixel 979, and the Moon via the space view (SV) at 11.4° AOI, EV pixel 24 [17]. These two points provide a limited description of the complete RVS function. In addition, lunar calibrations of MODIS ocean-color red and near-infrared bands cannot be performed directly, because these bands saturate when viewing the Moon. Conversely, there is no onboard capability to track changes in polarization sensitivity of the MODIS instruments [18]. Prelaunch measurements showed polarization amplitudes increasing toward the higher mirror AOIs and adding up to 2% for most ocean-color bands, except for band 8 (412 nm), where the amplitude was 5%; band 9 (443 nm), with the amplitude of 3%; and band 16 (869 nm) at 2.5% amplitude [19]. As an example, based on these prelaunch measurements and estimates of atmospheric polarization over the ocean, the polarization correction to MODIS TOA radiances at 412 nm is up to 3% of the total signal. In MODIS–Terra, seasonal and hemispherical trends in derived ocean-color products and variations in sensor response along the scan indicate its polarization sensitivity is changing, and it varies unevenly between the two mirror sides [5]. MODIS–Terra ocean-color data furthermore exhibit significant detector striping up to 10% in 412 nm water-leaving radiances [5]. For ocean-color bands, system-level calibration of each band's 10 detectors is operationally traced using SD data. Its independent verifications at SV AOI with lunar irradiances generally indicate detector estimates are different between these calibrators [17]. Mirror-side ratio trending is accomplished using spectroradiometric calibration assembly (SRCA) and EV data.

This paper describes a vicarious recharacterization approach addressing instrument on-orbit degradation when onboard calibration sources become insufficient to resolve sensor characterization issues, as in the case of MODIS–Terra. The approach uses EV data over oceans as a substitute, because in oligotrophic waters and clear atmospheres, expected instrument response can be fairly reliably modeled. A detailed description of the method is provided, which complements its previous introduction in [5], as well as results to demonstrate the improvement in ocean-color retrievals over the MODIS–Terra mission lifetime. The approach builds on the previous work undertaken to improve on-orbit radiometric calibration of the Modular Optoelectronic Scanner [20] and Landsat-7/Enhanced Thematic Mapper [21]. The concept closely follows ocean-color vicarious calibration [14], but instead of using sparse *in situ* ground measurements to model expected TOA signal, observations are used from another well-calibrated global sensor. The approach is therefore called a cross calibration. The ocean surface contribution is derived here using SeaWiFS data. The benefit of using SeaWiFS is twofold: SeaWiFS operations span the entire lifetime of Terra, and SeaWiFS is radiometrically well characterized and not sensitive to polarization [8]. Sensor-to-sensor matchups result in large calibration datasets with significant statistical representations of MODIS viewing and solar geometries for all spectral bands, mirror sides, and detectors.

MODIS issues such as RVS and polarization sensitivity are closely intertwined, and their separation and detailed characterization critically depend on the availability of such comprehensive datasets. RVS and polarization sensitivity are both functions of AOI on the mirror. They can yet be isolated, because RVS varies uniformly along the scan, while polarization of EV radiation that is incident on the mirror also varies with solar geometry and can be largely modeled independently. Furthermore, the approach extracts long-term calibration discrepancies between instruments as it ties the calibrated sensor to the temporal trend of the baseline mission. Therefore, MODIS–Terra, after the cross calibration with SeaWiFS, will contain SeaWiFS long-term trends and cannot create an independent climate data record. Nevertheless, it may be possible to disentangle MODIS RVS, polarization sensitivity, and mirror-side and detector corrections from SeaWiFS long-term trends. The potential solution to this issue is presented in Section 6.

2. Impact of Moderate Resolution Imaging Spectroradiometer–Terra Uncertainties on Ocean-Color Data

Detailed documentation describing MODIS–Terra onboard calibration is contained on the website of the MODIS Characterization Support Team (MCST) [22]. Here, limitations of this calibration are highlighted in order to explain the need for a complementary approach to on-orbit Terra calibration [5].

There are two events in MODIS–Terra history that significantly affect the performance of its derived ocean-color products. The first event occurred before the mission launch during an instrument characterization activity. During thermal vacuum testing, a portion of the nadir aperture door became overheated [23]. This resulted in the evaporation of a strip of paint (surface epoxy) from the door, which was about 0.6 m long and 0.02 m wide. The evaporation sprayed the inside of the scan cavity and the mirrors. Because of the vacuum, the spray traveled along the "line of sight" from the nadir aperture door. The scan mirror was rotating at the time, hence both sides of it were contaminated as was the fold mirror in the optical path from the scan mirror and the SRCA fold mirror. The blackbody was also impacted. In addition, a sample witness mirror was covered by the spray that was later used for practice cleaning of optical surfaces. The mirrors were cleaned, but not all contamination was removed completely, particularly at the edges of the scan mirror. There were differences in the cleaning outcome between the two sides of the scan mirror. The RVS was not subsequently recharacterized, thus its state at launch is not known exactly. This is important, because once on orbit, the shape of the MODIS prelaunch RVS is used to calibrate the instrument. MODIS–Terra onboard calibrations confirm that the radiometric sensitivities of the two mirror sides are different and have been changing over the course of the mission (see Fig. 1). Also, the trends at SV and SD AOIs diverge unevenly. These differences indicate that the shape of the RVS may be changing on orbit.

The second meaningful event occurred while on orbit in May 2003 during Terra SD calibration. During the procedure, the SD door was commanded to the full open position, but the SD screen remained closed, although the drive motor moved throughout its dynamic range. A recovery plan was implemented in July 2003, as a result of which the SD door remains permanently open while the screen is permanently closed. The opened SD door is causing increased degradation in reflective properties of the SD plate and possibly of the scan mirror. Although changes in the SD are tracked by the SD stability monitor (SDSM), its characterization capabilities may be degrading because of the rapidly decreasing SD reflectivity and the smaller signal, which is now available for its calibration.

Figure 1 shows change in MODIS–Terra and MODIS–Aqua calibration of band 8, 412 nm. Radiometric sensitivity of this Terra band has deteriorated by over 40% since launch. Band 8 has the highest radiometric change in MODIS, followed by the other ocean-color visible and near-infrared bands. The figure illustrates that the two sides of the MODIS–Terra mirror have been degrading differently and that the RVS between the SD and SV AOIs has been varying unevenly. MODIS–Aqua responsivity adjustments in band have also been large. However, in contrast to Terra, the RVS of Aqua has been changing relatively smoothly through time, and the two mirror sides have been fairly uniform. The prelaunch mirror contamination and in-flight permanent opening of

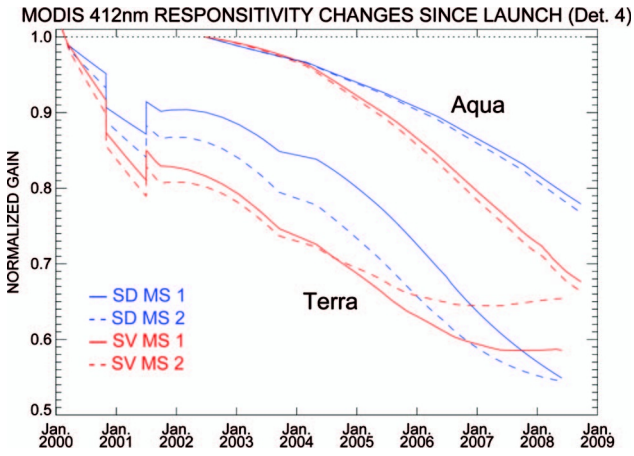

Fig. 1. On-orbit direct calibration results for MODIS–Terra and Aqua band 8, 412 nm. Band 8 response has been degrading the most on both platforms. Instrument radiometric sensitivities are tracked by Sun observations relayed by the SD and Moon observations through the SV port. Results are shown for two sides of the MODIS scan mirror, mirror-side 1 (MS1) and mirror-side 2 (MS2), and for detector 4 of band 8. SD trends are corrected for degradation of the diffuser plate, which is assessed by the SDSM. MODIS–Terra calibration shift in late 2000 to mid-2001 is caused by the switch in electronics side from A to B and back to A. MODIS–Terra calibration version is 5.0.38.1c, and MODIS–Aqua version is 5.0.35.2a.

the SD door may have affected MODIS–Terra in unpredictable ways, which show in substantial and uneven instrument changes. It is likely that MODIS–Terra polarization sensitivity has also been changing, although it cannot be monitored with onboard calibrators.

The impact of MODIS–Terra calibration uncertainties on ocean-color products, C_a and L_w in band 9, 443 nm, is illustrated in Fig. 2. The figure compares long-term anomalies after removal of systematic seasonal trends in SeaWiFS (top row) and MODIS–Terra (bottom row) in ocean-color time series. The anomalies are obtained for oligotrophic global ocean, which normally exhibits stability over many years without large long-term drifts in C_a and L_w. The TOA radiances are processed consistently between the two sensors using their respective onboard calibrations, corresponding fixed vicarious gains per band [14], and the same atmospheric correction [5]. Derived water-leaving radiances are normalized to eliminate viewing and solar illumination differences between the sensors (nL_w). The normalization approximates the conditions of a nadir-viewing instrument with the Sun being at zenith in absence of any atmospheric loss, the Earth being at its mean distance from the Sun, and with corrections for the effects of the nonisotropic structure of the subsurface light field [24]. The time series is obtained by averaging global oligotrophic C_a and nL_w values from consecutive 9 km spatial and 4 day temporal datasets, which are sampled once a month through the lifetimes of both missions. SeaWiFS long-term trends are relatively flat, within 8% of C_a and 4% of blue wavelength nL_w. MODIS–Terra, on the other hand, displays a significant drift in calibration starting around the SD door event in mid-2003. The drift is approximately 40% in terms of C_a and 15% in terms of band 9 443 nm nL_w. These MODIS–Terra calibration trends are unacceptable for ocean-color applications, as they significantly exceed a 5% uncertainty in blue-band water-leaving radiances.

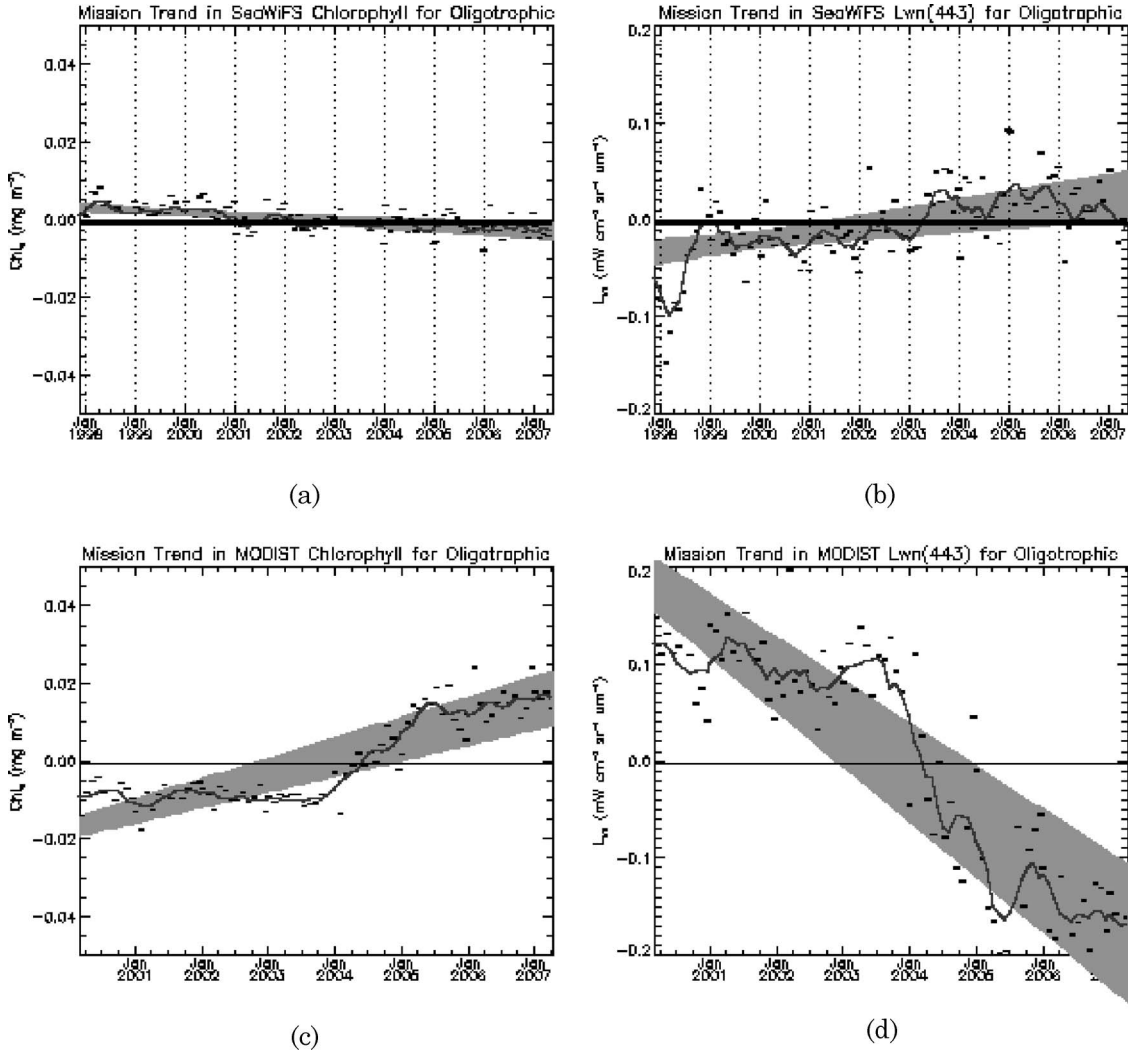

Fig. 2. (a), (c) Time series of chlorophyll-a concentrations, and (b), (d) normalized water-leaving radiances (nL_w or L_{wn}) for (a), (b) SeaWiFS and (c), (d) MODIS–Terra. The time series represent anomalies away from systematic yearly trends in oligotrophic global ocean. They are obtained by averaging sensor 4 day coverage sampled in monthly intervals through the lifetimes of both missions.

3. Cross-Calibration Methodology

The cross-calibration method described in this paper is based on modeling the TOA signal that should be measured by a polarization-sensitive instrument over oceans in presence of clear atmosphere and case 1 waters [25]. The prediction estimates the components of the Stokes vector exiting the TOA, $\mathbf{L}_t = [L_t, Q_t, U_t, V_t]^T$, which defines the total radiance (L_t) and the radiances due to linear (Q_t and U_t) and circular (V_t) polarization. The current prediction assumes the polarization of the visible TOA signal is solely due to atmospheric polarization and the specular reflection of the sunlight from the ocean surface, the sun glint. The contribution of surface foam and subsurface upwelled radiance to the TOA polarization is neglected. Additionally, the circular polarization of the atmosphere, V_t, is assumed to be insignificant [26]. The modeling of the total radiance, L_t, is founded on the methodology developed for ocean-color vicarious calibration [14,27]. However, unlike in the vicarious calibration, which uses *in situ* surface measurements, the known water-leaving radiances come from a baseline satellite sensor. The baseline nL_w compose a time series of sufficient length, consistency, reliable calibration, and global coverage to encompass the duration of the mission to be calibrated, thus producing a comprehensive matching series. Each dataset at each point in time in the series contains a broad global representation of viewing and solar geometries of the calibrated instrument, which enables the separation of RVS from polarization sensitivity. The radiances due to linear polarization of the atmosphere, Q_t and U_t, are modeled using the radiative transfer theory and are tabulated for discrete viewing and solar geometry angles or are evaluated *a priori*, as for the sun glint [2]. The actual signal measured by the instrument is then regressed against the prediction and unknown gain and polarization sensitivity are extracted.

A. Operational Vicarious Calibration

The vicarious calibration process for ocean-color data is described in detail in [14]. Its purpose is to reduce the uncertainty of the sensor direct calibration and its data processing algorithm. It results in single vicarious calibration gains for each band averaged throughout the mission lifetime, assuming temporal drift in instrument radiometric sensitivity is accounted by onboard calibrations. The vicarious calibration is effectively an inversion of the forward ocean-color processing algorithm [14]. The TOA total signal for a wavelength λ is decomposed as follows:

$$L_t(\lambda) = [L_r(\lambda) + L_a(\lambda) + t_{dv}(\lambda)L_f(\lambda) + t_{dv}(\lambda)L_w(\lambda)]t_{gv}(\lambda)t_{gs}(\lambda). \quad (1)$$

The contribution from the atmosphere is decoupled into gaseous absorption, where $t_{gs}(\lambda)$ and $t_{gv}(\lambda)$ correspond to radiance losses along the paths from the Sun to the surface and from the surface to the sensor [28]; into molecular scattering, $L_r(\lambda)$ [29,30]; and to aerosol scattering and absorption, $L_a(\lambda)$, which includes molecule–aerosol interactions [2]. The expression $L_f(\lambda)$ represents radiance contribution from the surface foam [2,31,32]. The term $t_{dv}(\lambda)$ accounts for diffuse transmittance along the path from surface to satellite [28]. Gaseous absorption is modeled using daily concentrations of individual gases in the atmosphere. Molecular, or Rayleigh, scattering is accurately predicted in advance, using vector radiative transfer, and is tabulated per solar and viewing geometries and wind speeds [29,30]. Aerosol types are also modeled, using Mie theory, and are tabulated but cannot be predicted *a priori* for ever-changing local atmospheric conditions. The primary unknowns in Eq. (1) are therefore $L_a(\lambda)$ and $L_w(\lambda)$. During the processing, pairs of bounding aerosol models are selected, depending on instrument measured reflectances in two bands in the near-infrared part of the spectrum [2]. The first step in the vicarious approach is therefore a relative calibration of these near-infrared bands to accurately retrieve the aerosol models, where the longer-wavelength band is kept at its direct onboard calibration value [14]. The next step is calibration of the visible bands. Here the aerosols are picked based on the established near-infrared relative calibration, and the surface contribution is determined using ground-measured *in situ* water-leaving radiances. A marine optical buoy (MOBY) has been a well-maintained vicarious calibration source since just before the SeaWiFS launch in 1997 [33,34]. The vicarious gains are derived from comparisons between vicarious and measured TOA radiances, and once established, they are applied in the operational processing of SeaWiFS and MODIS data.

B. Total Radiance Modeling L_t

In the cross-calibration process, Eq. (1) is used to model the total radiance, $L_t(\lambda)$, the first component of the Stokes vector exiting the TOA over ocean, $\mathbf{L_t}(\lambda)$. Instead of using MOBY measurements, $L_w(\lambda)$ in Eq. (1) is estimated from corresponding normalized water-leaving radiances from a baseline mission. Normalized water-leaving radiances are assumed to be independent of transient observation conditions and transferable among different instruments once adjusted for the instrument's individual relative spectral responses (RSRs). There are three options for deriving $L_a(\lambda)$:

1. Cross calibration of visible bands only. Aerosol contribution to the TOA signal, $L_a(\lambda)$, is predicted using the near-infrared bands of the sensor that is being calibrated. This assumes that the operational calibration of the near-infrared bands is adequate, encompassing direct onboard and vicarious calibrations, and that the operational prelaunch characterization of their polarization sensitivities is also valid. Temporal degradation, RVS, and polarization correction are then derived for the visible bands only.

2. Concurrent cross calibration of near-infrared and visible bands. Visible-band nL_w from the baseline sensor is used in concert with baseline estimates of the aerosol load. Here both nL_w and aerosol optical thickness (AOT) are assumed to be independent of transient observation conditions and transferable between instruments once adjusted for the instrument's RSRs. Spectral distribution of baseline AOTs defines a pair of bounding aerosol models. The AOTs, aerosol model scattering properties, and observation and solar geometries from the calibrated sensor are used to derive its aerosol radiances, $L_a(\lambda)$. This enables characterization of temporal degradation, RVS, and polarization sensitivity of the visible and near-infrared bands simultaneously.

3. Relative cross calibration of the near-infrared bands and full cross calibration of the visible bands. From the baseline mission, visible-band nL_w are used jointly with aerosol models defined by their Ångström exponent. Similarly to the vicarious calibration, the two-step procedure first performs the relative cross calibration of the near-infrared bands and then the full cross calibration of the visible bands. For the near-infrared bands, the longer-wavelength band is kept at its direct onboard calibration and prelaunch polarization sensitivity, so its L_a is unchanged, while the shorter-wavelength band L_a is predicted using the baseline aerosol model. Temporal degradation, RVS, and polarization correction are then derived for the shorter-wavelength near-infrared band and for all visible bands.

C. Measured Radiance Modeling, L_m

The radiance reflected from the ocean-atmosphere system can be strongly polarized, which affects polarization-sensitive instruments like MODIS. The degree of polarization of the modeled TOA radiances varies strongly with the scattering angle, typically between 0 and 70% at MODIS geometries [19]. Although the sensor's detectors measure mostly total radiance, this radiance is transformed by the prior action of the optical system, which is described by the following equation [26]:

$$\mathbf{L_m} = \mathbf{M}\mathbf{R}(\alpha)\mathbf{L_t}, \tag{2}$$

where

$$\mathbf{M} = \begin{bmatrix} M_{11} & M_{12} & M_{13} & M_{14} \\ \cdots & & & \cdots \\ \cdots & & & \cdots \\ M_{41} & \cdots & \cdots & M_{44} \end{bmatrix},$$

$$\mathbf{R}(\alpha) = \begin{bmatrix} 1 & 0 & 0 & 0 \\ 0 & \cos 2\alpha & \sin 2\alpha & 0 \\ 0 & -\sin 2\alpha & \cos 2\alpha & 0 \\ 0 & 0 & 0 & 1 \end{bmatrix}, \qquad \mathbf{L_t} = \begin{bmatrix} L_t \\ Q_t \\ U_t \\ V_t \end{bmatrix},$$

and wavelength λ is dropped for clarity from $\mathbf{L_m}(\lambda)$, $\mathbf{M}(\lambda)$, and $\mathbf{L_t}(\lambda)$. $\mathbf{M}(\lambda)$ is the Mueller matrix that characterizes instrument polarization sensitivity scaled by its gain. The Mueller matrix is defined relative to a reference plane fixed with respect to the instrument, while $\mathbf{L_t}(\lambda)$ is delineated with respect to a reference plane determined by the propagation direction of the light and the local vertical at ocean surface [26]. Hence the $\mathbf{L_t}(\lambda)$ vector has to be rotated, which is accomplished by the rotation matrix $\mathbf{R}(\alpha)$, where α is an angle between the two planes. At MODIS geometries, α is mostly 0° or ±180°, except around the very center of the scan at sensor azimuth discontinuity.

The total radiance measured by the detectors, i.e., the first element of the $\mathbf{L_m}$ Stokes vector, L_m, has contributions from the linear and circular polarization states of the incoming radiation, Q_t, U_t, and V_t. However, because molecular and aerosol scattering produces light largely linearly polarized, $V_t \sim 10^{-3}\ L_t$ [26], the circular polarization component is neglected:

$$\begin{aligned} L_m = {} & M_{11}L_t + M_{12}(Q_t \cos 2\alpha + U_t \sin 2\alpha) \\ & + M_{13}(-Q_t \sin 2\alpha + U_t \cos 2\alpha), \end{aligned} \tag{3}$$

where M_{11} is the instrument gain, and M_{12} and M_{13} are polarization sensitivities.

In the cross calibration, L_t are vicarious TOA total radiances modeled using Eq. (1). The rotation angle α is calculated *a priori* from the information on sensor viewing geometry and geographic coordinates of the imaged location. Linear polarization components Q_t and U_t are derived from vector radiative transfer simulations for molecular scattering in the atmosphere, glint scattering, and optionally for the 12 aerosol models used in the operational ocean-color atmospheric correction [30,35]. The Q_t and U_t components are computed *a priori* for the sun glitter and are parameterized for a wide spread of sensor and solar geometries, atmospheric pressures, and wind speeds in Rayleigh lookup tables and for the geometries and AOTs in aerosol tables.

D. Deriving Instrument Characterization

When L_m in Eq. (3) is replaced with the actual MODIS TOA measurements, L_m^m, the equation has three unknowns: M_{11}, M_{12}, and M_{13}. The goal of the cross-calibration process is to extract those unknowns simultaneously at each single point in the sensor time series. In the current implementation, M_{11}, M_{12}, and M_{13} are derived independently for each day in the time series and separately for each spectral band, mirror side, and detector. To be precise, the unknowns in the time series are expressed as functions of the spectral band (λ), mirror side (m), detector number, (d), and time (t) as $M_{11}^{md}(\lambda,t)$, $M_{12}^{md}(\lambda,t)$, and $M_{13}^{md}(\lambda,t)$. M_{11}, M_{12}, and M_{13} are also defined as functions of AOI on the mirror expressed in terms of pixel number (or frame number) of EV data. Here M_{11}, M_{12}, and M_{13} are defined as polynomial functions of pixel number:

$$M_{1i} = M_{1i,0} + M_{1i,1}p + \ldots + M_{1i,n}p^n, \qquad i \in \{1,2,3\}, \tag{4}$$

where p is the EV pixel number, $p \in \{1, \ldots, 1354\}$ for MODIS ocean-color bands, and n is the degree of the polynomial. Optionally, Eq. (3) can be solved within k consecutive pixel ranges along the scan, which will give k independent solutions $M_{11,i}$, $M_{12,i}$, and $M_{13,i}$, $i \in \{1, \ldots, k\}$.

E. Result Interpretation

In the cross-calibration process, M_{11} is a relative correction. The along scan change in derived M_{11} defines the residual RVS on top of the operational mirror characterization. The relative change over time in M_{11} magnitude at any given mirror AOI represents the long-term temporal trend on top of the operational onboard calibration. The absolute magnitude of M_{11} is partly dependent on the RSR conversions between the bands of the baseline and calibrated sensors, which are modeled and may not be very accurate. To limit the uncertainties in derived ocean-color products after the cross calibration, a new vicarious calibration is applied using MOBY *in situ* measurements.

M_{12} and M_{13} identify the instrument's absolute polarization sensitivity. They vary with the AOI on the mirror. M_{12} and M_{13} can be normalized to represent polarization sensitivities of a calibrated instrument, m_{12} and m_{13}:

$$m_{12} = \frac{M_{12}}{M_{11}}, \qquad m_{13} = \frac{M_{13}}{M_{11}}, \tag{5}$$

so that the calibrated and polarization corrected radiance is retrieved as

$$L_t = L_m/M_{11} - m_{12}(Q_t \cos 2\alpha + U_t \sin 2\alpha) - m_{13}(-Q_t \sin 2\alpha + U_t \cos 2\alpha). \tag{6}$$

Operational m_{12} and m_{13} values were derived during prelaunch polarization sensitivity characterizations for a calibrated instrument, i.e., $M_{11} = 1$, and have been kept constant through time. In the cross-calibration process, absolute values of M_{12} and M_{13} are allowed to trend over time through the time series as polarization sensitivity of the instrument changes. The magnitudes of m_{12} and m_{13} describe the instrument polarization response where its polarization amplitude is defined as [19]

$$p_a = \sqrt{m_{12}^2 + m_{13}^2}. \tag{7}$$

The unknowns, M_{11}, M_{12}, and M_{13}, therefore address diverse issues of instrument characterization and calibration: long-term temporal trends, RVS, polarization sensitivity, striping, and banding. If the unknowns are defined as polynomials of a pixel number, Eq. (3) constitutes an overdetermined set of linear equations. A least squares solution to these equations can be sought using a variety of algorithms such as robust singular value decomposition, multiple linear regression, or multidimensional function minimization like a downhill simplex method [36]. Machine learning approaches can also be implemented, which proved useful in cross calibrating ocean-color data on the level of water-leaving radiances [37].

4. Cross-Calibration Implementation

The cross-calibration uses a time series of large globally distributed sensor datasets from the two missions. It provides significant statistical representations of instrument viewing and solar geometries for all spectral bands, mirror sides, and detectors. The time series is composed of individual whole days of MODIS–Terra global coverage sampled at monthly intervals throughout the Terra lifetime. For each day in the time series, the cross calibration is in practice composed of four operational stages:

1. Matching of MODIS pixels with SeaWiFS nL_w (and AOT or Ångström for options 2 or 3, Section 3.B).
2. Inverse processing of MODIS to bring SeaWiFS nL_w to the TOA and output modeled pixel Stokes vectors, $[L_t, Q_t, U_t, 0]^T$, at MODIS wavelengths and MODIS solar and viewing geometries.
3. Screening TOA pixels and inserting them into datasets encompassing radiance pairs $([L_t, Q_t, U_t, 0]^T, L_m^m)$ and ancillary information, including rotation angle α, pixel mirror side, detector number, along-scan number, pixel date, geographic coordinates, solar and viewing geometries, and glint reflectance.
4. Solving an overdetermined set of linear equations to derive M_{11}, M_{12}, and M_{13} per band, mirror side, and detector.

The first step in the cross-calibration matches in space and time MODIS pixels with SeaWiFS level-2 pixels or MODIS pixels with SeaWiFS level-3 bins. The bins contain spatially and temporally averaged pixels in a global equal area grid of standard size [38]. Matching of individual pixels between sensors is computationally more involved. It is implemented using a k-dimensional tree search mechanism in spherical geographic coordinates [39]. The current implementation, however, uses SeaWiFS level-3 bins averaged within 9 km and 9 days centered on the day of MODIS analysis. The use of bins is preferred in order to eliminate noise and uncertainties associated with matching individual pixels between the sensors. It also averages out SeaWiFS potential residual RVS and mirror-side differences as well as stray light and atmospheric correction uncertainties. Case 1 water is used in the cross calibration by selecting global open-ocean coverage over 1000 m in depth. Only these bins that meet the standard level-3 mask criteria (http://oceancolor.gsfc.nasa.gov/VALIDATION/flags.html)

and contain a significant number of averaged pixels and swaths are applied. Bins are further restricted to those with maximum AOT at 865 nm below 0.15, a C_a threshold of 0.15 mg/m^3, and coefficients of variation for AOT and C_a below 0.15. These screening criteria approximately correspond to the standards used in the vicarious MOBY-based calibration [14]. Because the cross-calibrated instruments have different spectral bands, their band radiances are adjusted. This is accomplished on the level of SeaWiFS nL_w and AOT products after the screened matches are extracted and before the pixels are passed to the MODIS inverse processing. The nL_w conversion uses bio-optical models of case-1 marine reflectance [40,41]. SeaWiFS level-3 nL_w are converted from nominal band RSR, ±5 nm from the band center, to full-band RSR nL_w of MODIS–Terra. SeaWiFS band 670 nm nL_w are used to model MODIS nL_w in both bands 13, 667 nm, and 14, 678 nm. To convert AOT between sensor bands, the Ångström power law is applied. It is accomplished using linear interpolation in the logarithmic wavelength and AOT space between pairs of adjacent bands.

The daily MODIS coverage and corresponding vicarious data files are applied in the subsequent inverse processing to generate modeled TOA Stokes vectors. A separate stage in the cross calibration examines all processed files, extracts valid pixels and their ancillary information, and accumulates the pixels in a final cross-calibration dataset. The pixels undergo a screening in case the inverse processing encountered a failure or warning due to the instrument navigation problems, atmospheric correction, stray light, high glint, or proximity to clouds and bright targets. A single day of MODIS daytime imaging encompasses approximately 140 files, where each file is a 5 min granule. The screening criteria decrease the number of granules to between 70 and 80 a day and to over 200,000 daily pixels, which represent an adequate global distribution of ocean data. There are individual cross-calibration datasets for each day in the Terra time series.

In the current implementation, M_{11}, M_{12}, and M_{13} are modeled as polynomial functions of the pixel number along the MODIS–Terra scan. M_{11} is represented by a cubic function and M_{12} and M_{13} by linear functions. The cubic function for M_{11} was selected through experience due to irregularity of RVS, as different fractions of the mirror surface are used in reflection. The polarization sensitivity along the scan is modeled by a simpler function, just using a linear fit, because of lower confidence in its derived values, and because prelaunch measurements showed its relatively linear behavior. M_{11}, M_{12}, and M_{13} are derived separately for each band, mirror side, and detector. MODIS high and moderate glint are avoided, i.e., pixels with glint reflection coefficient above 0.0001, because they contribute significantly to uncertainties in derived parameters. For all screened pixels, the following overdetermined set of linear equations is solved:

$$L_m^m = M_{11,0}L_t + M_{11,1}pL_t + M_{11,2}p^2L_t + M_{11,3}p^3L_t + M_{12,0}Q_t' + M_{12,1}pQ_t' + M_{13,0}U_t' + M_{13,1}pU_t', \tag{8}$$

where, for a given band, mirror side, and detector, L_m^m, L_t, Q_t', and U_t' are global sets of measured and modeled radiances; p is their corresponding EV pixel number; $Q_t' = Q_t \cos 2\alpha + U_t \sin 2\alpha$; and $U_t' = -Q_t \sin 2\alpha + U_t \cos 2\alpha$. Equation (8) is resolved using an outlier resistant multiple linear regression.

5. Cross-Calibration Results

Results for MODIS–Terra presented in this section are given for the cross calibration of the visible bands only. Simultaneous near-infrared and visible-band characterization using vicarious nL_w and AOT has so far produced unrealistic instrument characterization. The reasons may be that spatially and temporally averaged SeaWiFS AOT data lose the high rate of atmospheric variability in comparisons with MODIS, as well as they may encompass speckling from unidentified clouds and stray light in global area coverage. Also, ocean-color processing is optimized for nL_w extraction, while AOT and L_a often carry residual errors of the instrument and algorithm system calibration. The relative cross-calibration of near-infrared bands using baseline aerosol models defined by their vicarious Ångström exponents has also been attempted, but the results are inconclusive.

The current results are thus produced assuming MODIS near-infrared bands are accurately characterized using prelaunch, onboard, and operational vicarious gain calibration. These bands are used to extract aerosol contribution to the modeled TOA total radiance, L_t. TOA linear polarization components, Q_t and U_t, are modeled for atmospheric molecular and glint polarization only. MODIS–Terra is processed with a calibration lookup table (LUT) version 5.0.38.1c. This LUT is based on the MCST LUT version 5.0.38.1_OC2 but uses a revised near-infrared RVS calibration [5] and adjusted detector calibrations [42]. An excerpt from this LUT for band 412 nm is presented in Fig. 1. The derived gain, M_{11}, is therefore relative to this calibration, and polarization sensitivity, M_{12} and M_{13}, are obtained in their absolute magnitude. SeaWiFS nL_w are processed using operational calibration version 200707 and operational algorithms. The time series of extracted characterization coefficients, M_{11}, M_{12}, and M_{13}, is plotted in Fig. 3 for the three blue bands, which show the largest deviations in ocean-color products. The M_{11} gain is actually presented as its inverse, $1/M_{11}$, because the inverse defines the correction to the measured TOA radiances, L_m^m, and depicts the RVS function of the mirror. The coefficients M_{11}, M_{12}, and M_{13} are delineated at two mirror sides and at one detector, detector 4. They are also shown at three selected mirror AOIs: lunar SV AOI, nadir, and SD-equivalent AOI. There is noise in the derived

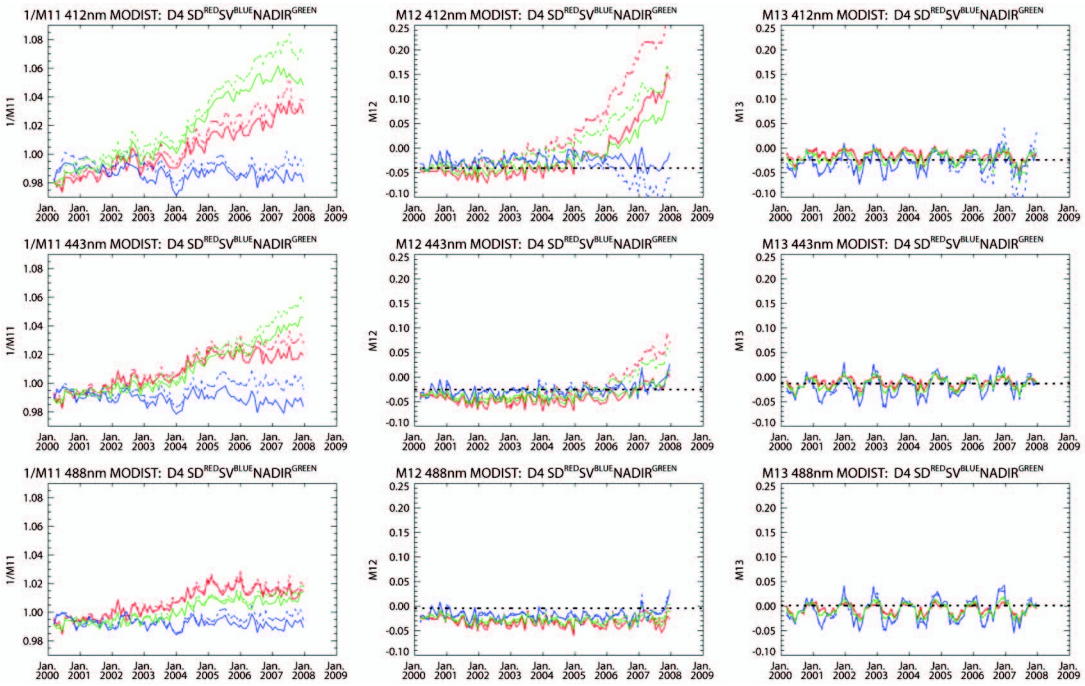

Fig. 3. Cross-calibration results for MODIS–Terra blue bands 8–10, 412, 443, and 488 nm, which showed the strongest discrepancies in derived ocean-color products. The results are gain $1/M_{11}$ and polarization sensitivities M_{12} and M_{13}, which are plotted through time for detector 4, both mirror sides, and at three mirror AOIs. Mirror-side 1 (MS1) is drawn in solid curve and mirror-side 2 (MS2) is in dotted curve. The three mirror AOIs are SV lunar equivalent shown in blue (EV pixel 24), nadir view in green (pixel 687), and SD equivalent in red (pixel 979). For M_{12} and M_{13}, prelaunch polarization sensitivities at nadir AOI are shown as black dotted lines.

coefficients, considering that they are extracted independently for each day in the time series. The noise is within 1–2% in the gain and is larger for the polarization sensitivity. However, beyond the noise, reasonable RVS and polarization patterns emerge.

The gain, $1/M_{11}$, in Fig. 3 shows that the calibration of MODIS–Terra is relatively stable over time at the SV AOI. At other AOIs, the gain changes over time, particularly increasing after the mid-2003 SD door event, which corresponds to strong reshaping of the mirror RVS function. There is also a difference between the two mirror sides where the spread in RVS is larger for mirror-side 2. Polarization sensitivity coefficient, M_{12}, in band 412 nm at mirror-side 2 shows a significant rise after the SD door event. M_{12} sensitivity intensifies from the beginning toward the end of MODIS scan, and this corresponds to increasing reflection footprint on the mirror. Polarization sensitivity of mirror-side 1 of band 412 nm similarly increases, but the process is delayed in time, as it is delayed in band 443 nm, and is almost indiscernible in band 488 nm. The polarization sensitivity coefficient, M_{13}, exhibits apparent seasonal patterns at similar magnitudes among the blue bands. This result appears erroneous as there are no obvious reasons why instrument polarization properties should vary seasonally. For most of the AOIs, M_{13} is associated only with the U_t linear polarization component, whereas M_{12} is associated with the Q_t component. It may be that the modeling assumptions do not adequately represent the polarization of the light that MODIS observes, particularly for linear $\pm 45°$ oscillations. Also, there can exist other unaccounted dependencies in the TOA signal. Because derived M_{13} coefficients vary evenly around their prelaunch values, the following analyses lock M_{13} at its prelaunch magnitude for all bands, and only M_{11} and M_{12} are treated as unknowns and are extracted in the cross-calibration process. With a fixed M_{13}, rederived M_{11} and M_{12} coefficients are not appreciably different, and the magnitude of instrument characterizations they describe, the RVS and polarization sensitivity, is not changed discernibly.

Noise in the temporal trends of the gain, M_{11}, and polarization sensitivity, M_{12}, is reduced by fitting smooth functions of time. There are individual fitting functions per M_{11}, M_{12}, band, mirror side, detector, and at a number of mirror AOIs sufficient to reproduce the extracted RVS patterns. Smoothed polarization sensitivities obtained early in the mission are similar to prelaunch measurements and less than 2% different. The smoothing of the gain is derived on top of onboard calibration trends. The resultant temporal gain distribution is therefore partly shaped based on the accuracy and consistency of the onboard calibration. To obtain all subsequent results, fifth degree polynomials are used in the smoothing. Nevertheless, locally adaptive smoothing filters, such as Savitzky–Goley, have given good results and may be preferred in the future [43].

Figure 4 displays $1/M_{11}$, M_{12}, and M_{13} for the blue bands along the MODIS scan and as functions of time

where the time progression is plotted with different colors. Mirror-side 1, detector 4 is shown in the top three rows in Fig. 4, and mirror-side 2, detector 4 is shown in the three bottom rows. As per the cross calibration, band 8, 412 nm, on MODIS–Terra has the most pronounced RVS differences on top of the

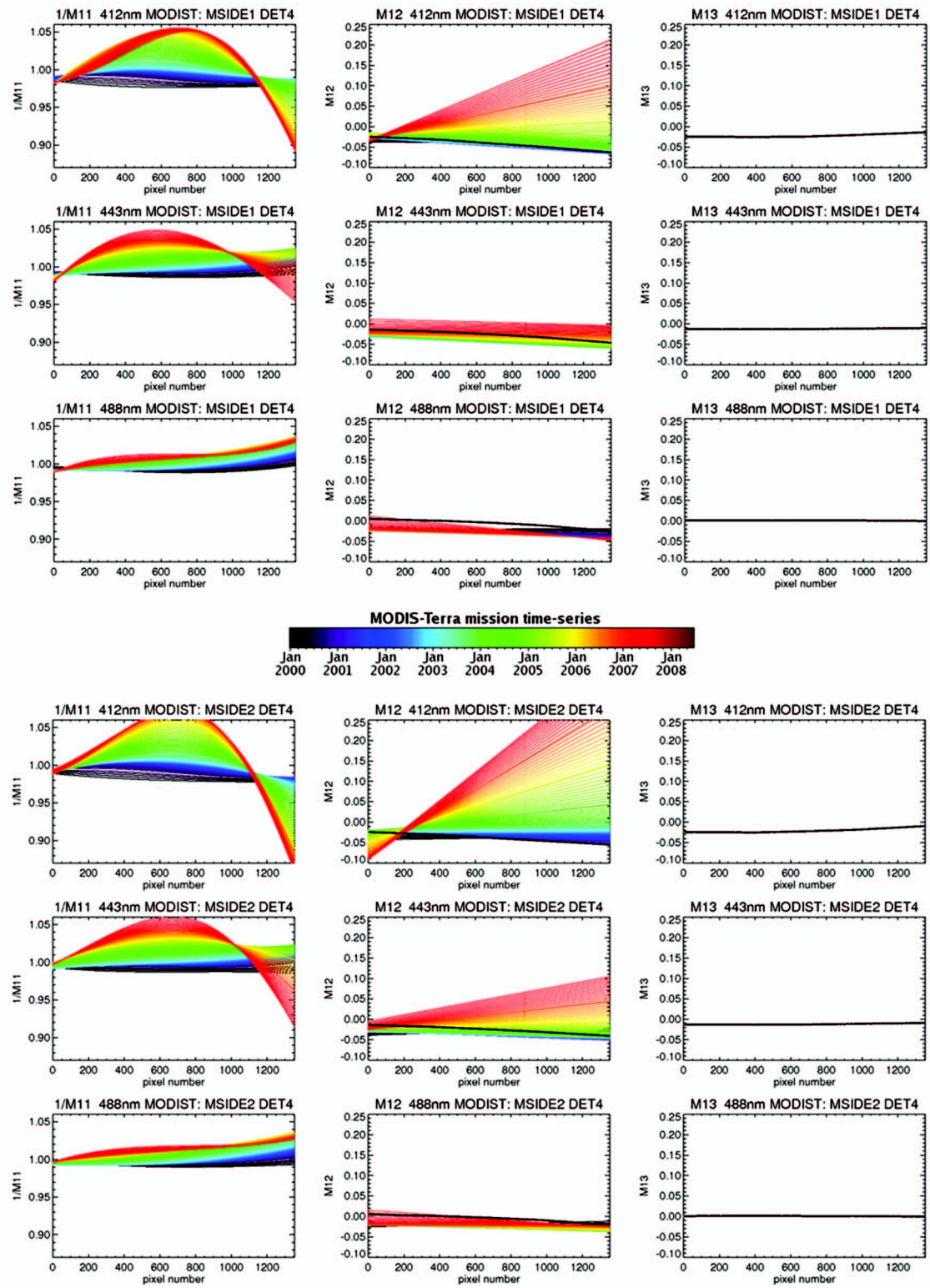

Fig. 4. Temporally smoothed cross-calibration results along MODIS scan for the blue ocean-color band RVS, $1/M_{11}$, and polarization sensitivities, M_{12}. The results are derived assuming operational prelaunch M_{13} values and are shown for detector 4 and two mirror sides, mirror-side 1 (MS1) in the top three rows and mirror-side 2 (MS2) in the bottom three rows. The colors illustrate progression in time from black/dark purple at the beginning of Terra mission imaging in 2000 to red at the end of 2007. Black dotted lines in the M_{12} and M_{13} plots represent prelaunch polarization sensitivity measurements.

operational characterization and the most varying polarization sensitivity. Changes in mirror-side 2 are larger than in mirror-side 1.

The shape of band 412 nm RVS has been significantly altered from less than 1% concave just after launch to strongly convex at the end of 2007. At the end of the time series, the cross-scan variability reaches approximately 7% between the beginning and the middle of the scan for mirror-side 1, and it is larger by approximately 2% for mirror-side 2. The variability at the end of the scan, where the entire surface of the mirror is used in reflection, curves significantly in the opposite direction. The RVS appears very stable at the lunar SV AOI, pixel 24, but it has changed by approximately 4% at SD AOI, pixel 979. Consequently, when applied to the TOA measurements 7 years into the mission, the cross calibration will increase MODIS–Terra response to unpolarized radiance at 412 nm (mirror-side 1, detector 4) in the middle of the scan by approximately 7% and will reduce its response by 10% at the end of the scan.

The polarization sensitivity of band 412 nm has been increasing from the beginning toward the end of the scan. This result is realistic, because the polarization sensitivity is expected to rise with AOI on the mirror. At the end of 2007 it reached approximately 20% at the end of the scan for mirror-side 1 and 30% for mirror-side 2. Polarization sensitivity of 30% at 412 nm over ocean at MODIS–Terra geometries corresponds to the correction of approximately 17% to the TOA-measured radiances, L_m^m. According to the cross-calibration results, band 9, 443 nm, behaves similarly to band 412 nm but with a temporal change in RVS that is smaller by a few percent and with 1/3rd the increase in polarization sensitivity. The variations in band 10, 488 nm, are even smaller: a 2–4% change over time in the RVS and a 1–4% change in polarization sensitivity that is dependent on the mirror side and mirror AOI. Extracted detector-to-detector variability, not shown in the figure, is within 2–3% for blue bands 412 and 443 nm, around 1% for band 488 and below 1% for the other visible ocean-color bands.

The green and red bands on MODIS–Terra have been changing on orbit significantly less than the blue bands. This result is shown in Fig. 5(a). The temporal variation of the RVS in green and red bands is between 1 and 2% and between 1 and 3% in polarization sensitivity. There is a 1 to 2% slope in the RVS from the beginning to the end of scan in those bands compared to the onboard calibration. Figure 5(b) demonstrates the result of the identical cross calibration performed for MODIS on the Aqua platform. In contrast with MODIS–Terra, MODIS–Aqua blue bands appear well characterized using operational onboard calibration. According to the cross calibration, MODIS–Aqua RVS has changed by less than 1%, and its slope departs from the onboard

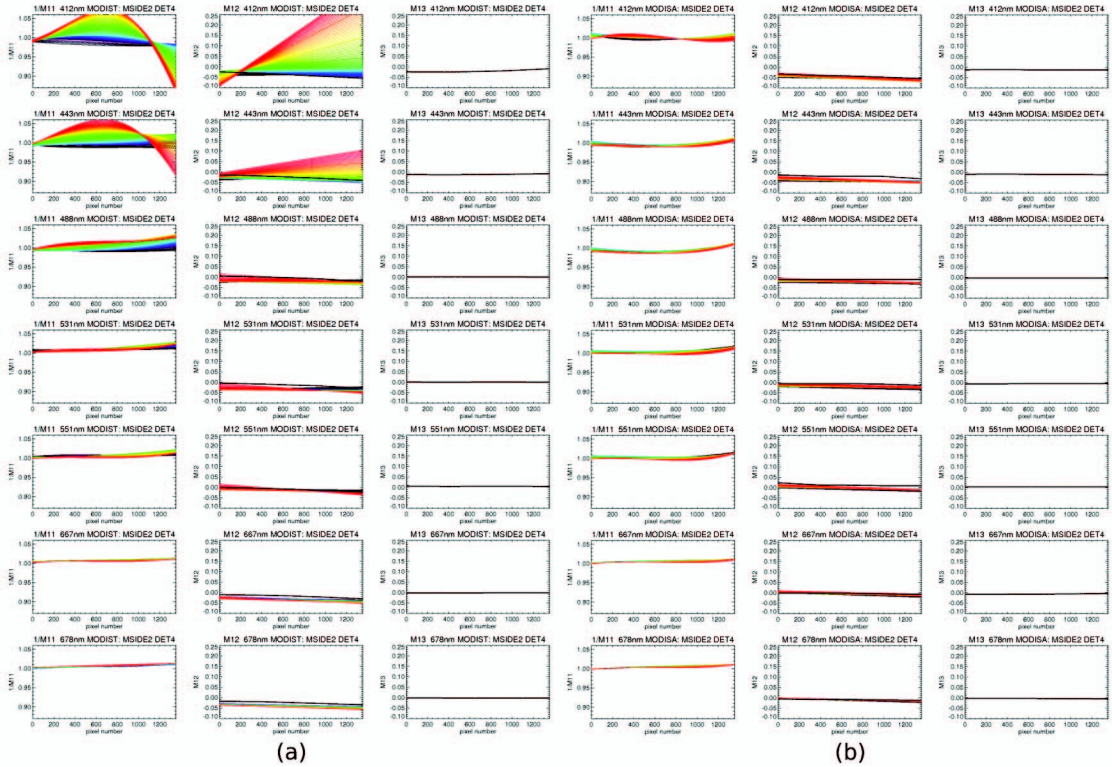

Fig. 5. Cross-calibration results for the two MODIS sensors on (a) Terra and (b) Aqua platforms. The same cross-calibration approach is applied for both instruments. The results are temporally smoothed and shown along scan for all seven visible ocean-color bands. RVS, $1/M_{11}$, and polarization sensitivity, M_{12}, are illustrated for mirror-side 2 and detector 4, where M_{13} are used at their operational prelaunch values. The colors depict progression in time from black/dark purple at the beginning of each mission to red at the end of 2007. Black dotted lines in the M_{12} and M_{13} plots represent respective prelaunch polarization sensitivity measurements.

calibration by 1%. Also, MODIS–Aqua polarization sensitivity has not been significantly changing on orbit, amounting to 2% maximum in the worst case of band 8.

Extracted MODIS–Terra characterization, long-term temporal trends, RVS, and polarization sensitivities have been tested using a time series of derived ocean-color products. Beforehand, ocean-color near-infrared and visible bands were vicariously recalibrated using the standard vicarious calibration procedure applied to MODIS cross-calibrated L_t. The near-infrared vicarious calibration should not change the gain, because in the current cross-calibration option, the near-infrared bands were not recharacterized. However, due to the cross-calibration adjustments, more scenes passed the screening criteria, and there was less scatter in the time series going into the gain derivation, which broadened the vicarious gain representation. The following vicarious calibration of the visible bands was performed with standard methodology with MOBY measurements.

There are a number of tests employed in the validation of ocean-color-derived products. One set of tests compares global, zonal, or regional time series between different instruments within overlapping ground coverage. Figures 6(a) and 6(d) show ratios of global oligotrophic ocean nL_w from MODIS–Terra and MODIS–Aqua over the joint mission lifetime and before and after the cross calibration. Cross-calibrated MODIS–Terra delivers nL_w, which are within 5% of Aqua values. This is similar to current SeaWiFS and MODIS–Aqua differences and is a significant improvement over previous discrepancies of 15% in the blue bands. Figures 6(b) and 6(e) delineate considerable advancement in the nL_w RVS and detector-to-detector calibration. The along-scan and detector response is quantified in terms of derived ocean products and obtained by comparing pixel-by-pixel deep-ocean global values against spatially and temporally averaged 7 day bins matched at each pixel location. Another form of validation consists of analyses of temporal anomalies in derived ocean-color time series on top of systematic yearly trends, as shown for SeaWiFS and Terra in Section 2. Oligotrophic waters exhibit stability over periods of many years without large long-term drifts in nL_w or C_a. These drifts are obvious before the cross calibration and diminish after the cross calibration is applied, which is illustrated in Figs. 6(c) and 6(f).

6. Discussion and Conclusions

The paper presents a vicarious calibration method for ocean-color satellite instruments, which is applicable when onboard sensor characterization capabilities become degraded. The method can extract long-term sensor radiometric trends as well as RVS and polarization sensitivity per spectral band, mirror side, and detector. Instead of onboard calibrator measurements, the characterization uses EV data over open ocean. These data are matched against the modeled TOA signal that the instrument is expected to observe. Ocean surface properties are modeled using data from another stable global satellite

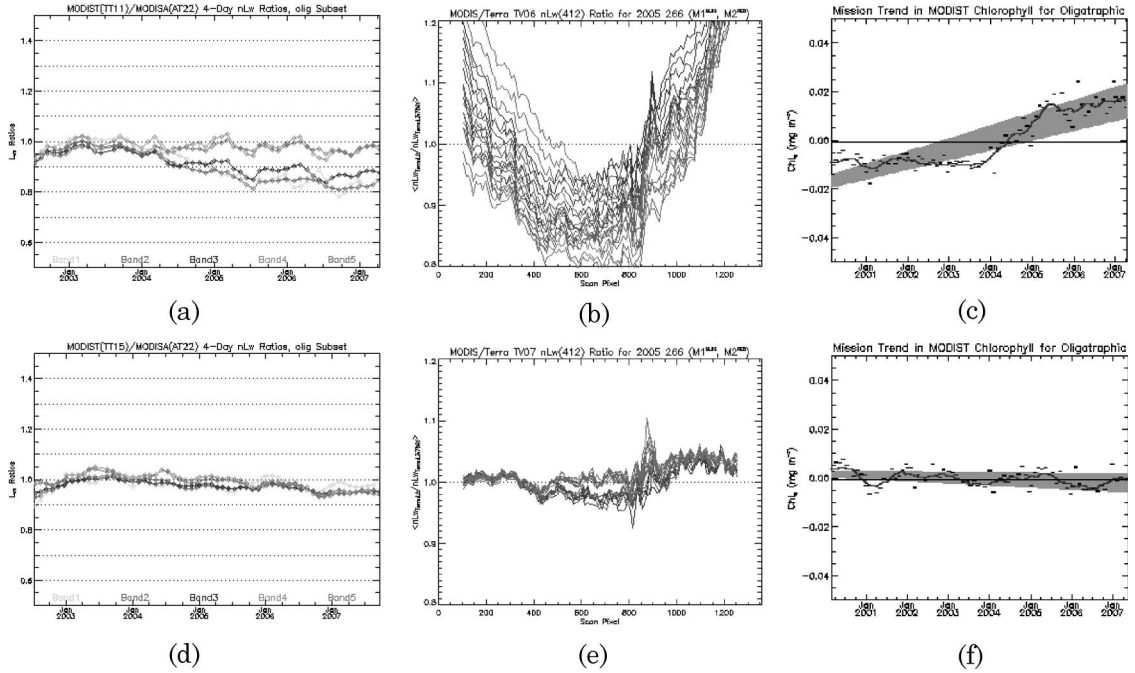

Fig. 6. Results of MODIS–Terra validation of derived ocean-color products (a)–(c) before and (d)–(f) after application of the cross calibration. (a), (d) The first column shows time series of ratios of normalized water-leaving radiances from MODIS–Terra and MODIS–Aqua for the blue and green bands. (b), (e) The second column demonstrates along-scan trends of RVS and detector variabilities in terms of normalized water-leaving radiances in band 8, 412 nm. (c), (f) The third column illustrates chlorophyll-a concentration anomalies away from systematic yearly trends in the oligotrophic ocean.

instrument. Atmospheric aerosol types and concentrations are currently modeled using the calibrated instrument itself and by assuming operational characterization of its near-infrared bands.

The strategy proved effective in deriving RVS and polarization sensitivity for MODIS–Terra by cross calibrating it with SeaWiFS normalized water-leaving radiances. The ocean-color blue bands, which carry the strongest degradation on MODIS–Terra, receive the most meaningful improvement from the cross calibration. Nevertheless, there are many concerns with the approach that should be addressed. They include the long-term availability of consistent well-calibrated time series, such as the one from SeaWiFS, which is needed for the cross calibration, as well as uncertainties associated with modeling the TOA signal.

The basis for the cross-calibration approach is the availability at any given point in time of comprehensive global datasets covering a broad range of viewing and solar geometries for the sensor that is being calibrated. The 10 year time series of nL_w from SeaWiFS has been used as a template for many studies of global and regional ocean biogeochemistry. The SeaWiFS instrument is, however, aging, and its orbit is decaying with the initial noon-descending node drifting eastward toward the afternoon at an accelerating rate. This causes increased concerns with SeaWiFS's state of health and uncertainties in SeaWiFS calibration associated with its growing temperature sensitivity. If SeaWiFS stops being a viable option for global baseline ocean color, the cross-calibration studies with MODIS–Aqua show that Aqua could replace SeaWiFS, because its RVS and polarization sensitivities have not been changing nearly as much as on MODIS–Terra, see Fig. 5. However, MODIS–Aqua is still a polarization-sensitive instrument, and its age or an event on orbit may cause it to degrade more rapidly. As an alternative, it may be feasible to use monthly nL_w climatologies or to model global oligotrophic nL_w based on chlorophyll climatologies [44] with the assumption that there are no climatic bio-optical changes in those kinds of waters.

There are significant uncertainties associated with modeling the TOA signal in ocean-color bands. The first assumption put forward in this analysis stipulates that the polarization of the light on the TOA over oceans is only due to the atmosphere and the specular reflection of the sunlight from the ocean surface, though sun glint is largely avoided in the analyses. However, it has been measured that the polarization of the underwater upwelled radiance can be up to 60% depending on the viewing and solar geometries [45]. Secondly, the circular polarization component of the TOA signal is assumed minimal, and is ignored. The next assumption postulates that the linear polarization of the atmosphere is only caused by molecular scattering. Aerosol polarization effects in the open ocean are shown to be usually negligible [35]. Prior MODIS–Terra cross calibrations explored additional polarization effects due to aerosols introduced into the modeled Q_t and U_t components. Although the differences in the derived RVS were below 0.5%, the differences in the extracted polarization sensitivities were more significant. Future studies will examine aerosol models defined using full-vector Mie theory, which will impact total L_a and aerosol Q_t and U_t components. Incomplete modeling of the polarization state of the TOA signal may be the cause for the seasonal patterns extracted in the M_{13} polarization sensitivity factor for both MODIS–Terra and MODIS–Aqua.

SeaWiFS ocean-color time series, the basis for the cross calibration, has shown remarkable consistency over the 10 years on orbit [14]. SeaWiFS was cross calibrated against its own level 3, 9 day, 9 km global bins using the same methodology as for MODIS–Terra but assuming no polarization sensitivity of the instrument and applying stricter stray-light screening criteria than in the operational SeaWiFS binning. This simpler version of the cross calibration provided the estimate of SeaWiFS visible-band RVS and placed it below 0.5% cross-scan variability and down to 0.1% in band 670 nm. This perceived RVS is relatively small, potentially within the error of the regression, and becomes insignificant in level 3 averaged data.

Past efforts to simultaneously characterize MODIS visible and near-infrared bands failed to derive feasible cross-calibration results, particularly MODIS polarization sensitivities. This cross-calibration option uses SeaWiFS aerosol products in the modeling of the part of MODIS L_t associated with unknown aerosol types and concentrations. As discussed before, SeaWiFS aerosol properties may not be transferable to MODIS–Terra, because SeaWiFS vicarious calibration is not absolute. It bounds instrument calibration to a specific aerosol model, and it is optimized to accurately retrieve nL_w, not atmospheric properties. AOT products may incorporate other nonaerosol constituents such as residual sun glint and unidentified clouds. In addition, open-ocean atmospheric aerosol conditions evolve faster than surface bio-optics and may not be applicable within an hour's time, let alone over a 9 day 9 km average. The analysis of MODIS–Terra ocean-color products shows that there may be a potential long-term 1% drift in the near-infrared bands relative to each other, whereas band 869 nm AOTs appear very stable compared to SeaWiFS. Unfortunately, the relative cross calibration based on SeaWiFS aerosol models has not shown conclusive results. The visible-band cross calibration indicates, however, that the trends on top of the operational characterization decrease significantly at longer wavelengths. The drift should therefore be relatively small in the near-infrared range and within the uncertainty of the regression for these bands.

The major concern with the cross-calibration approach is that it ties the calibrated sensor to the long-term calibration trend of the baseline mission, although this is not an uncommon practice for other

disciplines. Therefore, MODIS–Terra, after the cross calibration with SeaWiFS, cannot create an independent climate data record. It can still be useful for global and regional studies by complementing other instruments and providing increased daily coverage and enhanced statistical confidence in extracted bio-optical parameters. It is anticipated that new MODIS–Terra cross calibrations can be executed operationally in monthly intervals. For dates in between the cross calibrations, linear interpolation of RVS and polarization sensitivity is performed. MODIS–Terra RVS and polarization sensitivity should probably be predicted into the future by keeping constant the last available fit, because the derived temporal trends are complex and mostly nonlinear. This depends on the temporal smoothing of the original raw trends. For some applications, like in the case of MODIS–Aqua cross calibration, it may be useful to isolate RVS, polarization, mirror-side, and detector characterization without imposing long-term trend from the baseline instrument. This goal is difficult, because the shape of RVS and polarization sensitivity, as well as mirror-side and detector-to-detector discrepancies themselves, vary through time. The solution can be to normalize derived RVS across the entire time series at a given mirror AOI, e.g., SD AOI, or to normalize it to a cross-scan average of 1. Actually, the time series of RVS for mirror-side 1 detector 1 would be normalized, and the other detectors and the mirror side would be adjusted relative to them. This would preserve the original temporal trend of the calibrated instrument, and the final vicarious calibration would fine-tune the band radiances to the desired magnitude.

This work was supported under the NASA Research Opportunities in Space and Earth Sciences (ROSES) 2006 calibration and validation solicitation funding.

References

1. M. J. Behrenfeld, E. Boss, D. A. Siegel, and D. M. Shea, "Carbon-based ocean productivity and phytoplankton physiology from space," Glob. Biogeochem. Cycles **19**, GB 1006 (2005).
2. H. R. Gordon and M. Wang, "Retrieval of water-leaving radiance and aerosol optical thickness over the oceans with SeaWiFS: a preliminary algorithm," Appl. Opt. **33**, 443–452 (1994).
3. D. Antoine and A. Morel, "A multiple scattering algorithm for atmospheric correction of remotely sensed ocean colour (MERIS instrument): principle and implementation for atmospheres carrying various aerosols including absorbing ones," Int. J.Remote Sens. **20**, 1875–1916 (1999).
4. B. C. Gao, M. J. Montes, Z. Ahmad, and C. O. Davis, "Atmospheric correction algorithm for hyperspectral remote sensing of ocean color from space," Appl. Opt. **39**, 887–896 (2000).
5. B. A. Franz, E. J. Kwiatkowska, G. Meister, and C. R. McClain, "Moderate Resolution Imaging Spectroradiometer on Terra: limitations for ocean color applications," J. Applied Remote Sens. **2**, 023525 (2008).
6. C. R. McClain, G. C. Feldman, and S. B. Hooker, "An Overview of the SeaWiFS Project and Strategies for Producing a Climate Research Quality Global Ocean Bio-optical Time Series," Deep-Sea Res. II **51**, 5–42 (2004).
7. W. E. Esaias, M. R. Abbot, I. J. Barton, O. B. Brown, J. W. Campbell, K. L. Carder, D. K. Clark, R. H. Evans, F. E. Hoge, H. R. Gordon, W. M. Balch, R. Letelier, and P. J. Minnett, "An overview of MODIS capabilities for ocean science observations," IEEE Trans. Geosci. Remote Sens. **36**, 1250–1265 (1998).
8. R. A. Barnes, R. E. Eplee, Jr., G. M. Schmidt, F. S. Patt, and C. R. McClain, "Calibration of SeaWiFS. I. Direct techniques," Appl. Opt. **40**, 6682–6700 (2001).
9. R. E. Eplee, Jr., F. S. Patt, R. A. Barnes, and C. R. McClain, "SeaWiFS long-term solar diffuser reflectance and sensor noise analyses," Appl. Opt. **46**, 762–773 (2007).
10. X. Xiong, K. Chiang, J. Esposito, B. Guenther, and W. Barnes, "MODIS on-orbit calibration and characterization," Metrologia **40**, S89–S92 (2003).
11. X. Xiong, W. Barnes, K. Chiang, H. Erives, N. Che, J-Q. Sun, A. Isaacman, and V. Solomonson, "Status of Aqua MODIS on-orbit calibration and characterization," Proc. SPIE **5570**, 317–327 (2004).
12. S. B. Hooker, W. E. Esaias, G. C. Feldman, W. W. Gregg, and C. R. McClain, "An overview of SeaWiFS and ocean color," NASA Technical Memorandum 104566, Vol. 1, S. H. Hooker and E. R. Firestone, eds. (National Aeronautics and Space Administration, Goddard Space Flight Center, 1992).
13. H. R. Gordon, "In-orbit calibration strategy for ocean color sensors," Remote Sens. Environ. **63**, 265–278 (1998).
14. B. A. Franz, S. W. Bailey, P. J. Werdell, and C. R. McClain, "Sensor-independent approach to vicarious calibration of satellite ocean color radiometry," Appl. Opt. **46**, 5068–5082 (2007).
15. B. A. Franz, P. J. Werdell, G. Meister, S. W. Bailey, R. E. Eplee, Jr., G. C. Feldman, E. Kwiatkowska, C. R. McClain, F. S. Patt, and D. Thomas, "The continuity of ocean color measurements from SeaWiFS to MODIS," Proc. SPIE **5882**, 58820W (2005).
16. X. Xiong, J-Q. Sun, W. Barnes, V. Salomonson, J. Esposito, H. Erives, and B. Guenther, "Multi-year on-orbit calibration and performance of Terra MODIS reflective solar bands," IEEE Trans. Geosci. Remote Sens. **45**, 879–889 (2007).
17. J-Q. Sun, X. Xiong, B. Guenther, and W. Barnes, "Radiometric stability monitoring of the MODIS reflective solar bands using the Moon," Metrologia **40**, S85–S88 (2003).
18. J-Q. Sun and X. Xiong, "MODIS polarization-sensitivity analysis," IEEE Trans. Geosci. Remote Sens. **45**, 2875–2885 (2007).
19. G. Meister, E. J. Kwiatkowska, B. A. Franz, F. S. Patt, G. C. Feldman, and C. R. McClain, "Moderate-resolution imaging spectroradiometer ocean color polarization correction," Appl. Opt. **44**, 5524–5535 (2005).
20. M. H. Wang and B. A. Franz, "Comparing the ocean color measurements between MOS and SeaWiFS: a vicarious intercalibration approach for MOS," IEEE Trans. Geosci. Remote Sens. **38**, 184–197 (2000).
21. C. Hu, F. E. Muller-Karger, S. Andrefouet, and K. L. Carder, "Atmospheric correction and calibration of LANDSAT-7/ETM+ imagery over aquatic environments: a multi-platform approach using SeaWiFS/MODIS," Remote Sens. Environ. **78**, 99–107 (2001).
22. X. Xiong and W. L. Barnes, "An overview of MODIS radiometric calibration and characterization," Adv. Atmos. Sci. **23**, 69–79 (2006).
23. E. Waluschka, NASA Goddard Space Flight Center, Code 551.0, Greenbelt, Maryland 20771 (personal communication, 2008).
24. A. Morel and G. Gentili, "Diffuse reflectance of oceanic waters. III. Implication of bidirectionality for the remote-sensing problem," Appl. Opt. **35**, 4850–4862 (1996).

25. A. Morel and L. Prieur, "Analysis of variations in ocean color," Limnol. Oceanogr. **22**, 709–722 (1977).
26. H. R. Gordon, T. Du, and T. Zhang, "Atmospheric correction of ocean color sensors: analysis of the effects of residual instrument polarization sensitivity," Appl. Opt. **36**, 6938–6948 (1997).
27. S. W. Bailey, S. B. Hooker, D. Antoine, B. A. Franz, and P. J. Werdell, "Sources and assumptions for the vicarious calibration of ocean color satellite observations," Appl. Opt. **47**, 2035–2045 (2008).
28. M. Wang, "Atmospheric correction of ocean color sensors: computing atmospheric diffuse transmittance," Appl. Opt. **38**, 451–455 (1999).
29. M. Wang, "The Rayleigh lookup tables for the SeaWIFS data processing: accounting for the effects of ocean surface roughness," Int. J. Remote Sens. **23**, 2693–2702 (2002).
30. M. Wang, "A refinement for the Rayleigh radiance computation with variation of the atmospheric pressure," Int. J. Remote Sens. **26**, 5651–5653 (2005).
31. R. Frouin, M. Schwindling, and P. Y. Dechamps, "Spectral reflectance of sea foam in the visible and near infrared: *in situ* measurements and remote sensing implications," J. Geophys. Res. **101**, 14361–14371 (1996).
32. K. D. Moore, K. J. Voss, and H. R. Gordon, "Spectral reflectance of whitecaps: their contribution to water-leaving radiance," J. Geophys. Res. **105**, 6493–6499 (2000).
33. S. W. Brown, S. J. Flora, M. E. Feinholz, M. A. Yarbrough, T. Houlihan, D. Peters, Y. S. Kim, J. L. Mueller, B. C. Johnson, and D. K. Clark, "The marine optical buoy (MOBY) radiometric calibration and uncertainty budget for ocean color satellite sensor vicarious calibration," Proc. SPIE **6744**, 67441M (2007).
34. D. K. Clark, H. R. Gordon, K. J. Voss, Y. Ge, W. W. Broenkow, and C. Trees, "Validation of atmospheric correction over the oceans," J. Geophys. Res. **102**, 17209–17217 (1997).
35. M. Wang, "Aerosol polarization effects on atmospheric correction and aerosol retrievals in ocean color remote sensing," Appl. Opt. **45**, 8951–8963 (2006).
36. W. H. Press, B. P. Flannery, S. A. Teukolsky, and W. T. Vetterling, *Numerical Recipes, the Art of Scientific Computing* (Cambridge University, 1986).
37. E. J. Kwiatkowska and G. S. Fargion, "Application of machine learning techniques towards the creation of a consistent and calibrated global chlorophyll concentration baseline dataset using remotely sensed ocean color data," IEEE Trans. Geosci. Remote Sens. **41**, 2844–2860 (2003).
38. J. W. Campbell, J. M. Blaisdell, and M. Darzi, "Level-3 SeaWiFS data products: spatial and temporal binning algorithms," NASA Technical Memorandum 104566, Vol. 32, S. B. Hooker, E. R. Firestone, and J. G. Acker, eds. (National Aeronautics and Space Administration, Goddard Space Flight Center, 1995).
39. I. Kalantari and G. McDonald, "A data structure and an algorithm for the nearest point problem," IEEE Trans. Softw. Eng. **SE-9**, 631–634 (1983).
40. A. Morel and S. Maritorena, "Bio-optical properties of oceanic waters: a reappraisal," J. Geophys. Res. **106**, 7163–7180 (2001).
41. M. Wang, B. A. Franz, R. A. Barnes, and C. R. McClain, "Effects of spectral bandpass on SeaWiFS-retrieved near-surface optical properties of the ocean," Appl. Opt. **40**, 343–348 (2001).
42. G. Meister, E. J. Kwiatkowska, and C. R. McClain, "Analysis of image striping due to polarization correction artifacts in remotely sensed ocean scenes," Proc. SPIE **6296**, 629609 (2006).
43. A. Savitzky and M. J. E. Goley, "Smoothing and differentiation of data by simplified least squares procedures," Anal. Chem. **36**, 1627–1639 (1964).
44. P. J. Werdell, S. W. Bailey, B. A. Franz, A. Morel, C. R. McClain, and S. B. Hooker, "The on-orbit vicarious calibration of ocean color sensors using a sea surface reflectance model," Appl. Opt. **46**, 5649–5666 (2007).
45. K. Voss, Physics Department, University of Miami, Coral Gables, FL 33124 (personal communication, 2008).